Visual Abstract

Quantitative description of low-cycle fatigue damage accumulation in contact interaction zone by local strain evolution

Yu. G. Matvienko
Mechanical Engineering Research Institute of the Russian Academy of Science (IMASH RAN). 4 M. Kharitonievsky Per., 101990 Moscow, Russia.
matvienko7@yahoo.com, https://orcid.org/ 0000-0003-2367-0966

V.S. Pisarev, S. I. Eleonsky
Central Aero-Hydrodynamics Institute named after Prof. N.E. Zhukovsky (TsAGI). 1 Zhukovsky Street, Zhukovsky 140180 Moscow Region, Russia.
VSP5335@mail.ru, https://orcid.org/0000-0002-5378-609X
juzzepka@mail.ru, https://orcid.org/0000-0003-4345-067X

I. N. Odintsev
Mechanical Engineering Research Institute of the Russian Academy of Science (IMASH RAN). 4 M. Kharitonievsky Per., 101990 Moscow, Russia.
INO54@mail.ru

ABSTRACT. The novel non-destructive method for quantitative description of low-cycle fatigue damage accumulation is expanded to a case of contact interaction in the stress concentration area. Investigated objects are plane aluminium specimens with the centred hole filled by cylindrical steel inclusion. The specimen is subjected to cyclic pull-push loading. The key point, that defines scientific novelty and powerfulness of the developed approach, consists of involving local deformation parameters as current damage indicators. Required strain values follow from distributions of two in-plane displacement components along the filled hole edge measured by reflection hologram interferometry. The data, which are derived at different stages of low-cycle fatigue for the single specimen, provide normalized dependencies of local strain values from number of loading cycle, which are a source of damage accumulation functions. These functions are constructed for the specimen with the filled hole and geometrically analogous specimen with the open hole. Obtained data quantitatively describe a difference in damage accumulation rates for two cases.

KEYWORDS. Damage accumulation; Local strain evolution; Reflection hologram interferometry.

OPEN ACCESS

Citation: Matvienko, Yu. G., Pisarev, V. S., Eleonsky, S. I., Odintsev, I. N., Quantitative description of low-cycle fatigue damage accumulation in contact interaction zone by local strain evolution, Frattura ed Integrità Strutturale, 62 (2022) 541-560.

Received: 27.06.2022
Accepted: 09.09.2022
Online first: 12.09.2022
Published: 01.10.2022

INTRODUCTION

Investigation of damage accumulation, fatigue crack initiation and growth, inherent in stress concentration areas of airplane structures, especially in a case of contact interaction, are of considerable interest [1–2]. Situations, when a fast crack growth is attributed to high-level elastic-plastic strains due to low-cycle fatigue near a filled hole, need special attention. The first stage of low-cycle fatigue damage accumulation is not visible. That is why a quantitative description of damage accumulation demands involving measured parameters at different stages of low-cycle fatigue.

Presently, the analysis of damage accumulation as well as subsurface macro-defect initiation and further crack growth predictions in various structures are mainly founded upon deformation, energy-based, phenomenological and micro-mechanical models, which include different variables responsible for damage initiation at different stages of fatigue loading [3]. In particular, fracture mechanics is widely used in failure analysis and fatigue life estimations [4–9]. The involved approaches are mainly based on finite element modelling. Some of them employ experimental determination of parameters, which are essential in the course of numerical simulation.

Necessity of various experimental investigations of fatigue damage accumulation, especially in the case of local elastic-plastic strains availability, is substantiated in Refs. (e.g. [2, 10–11]). Optics-based techniques appear to be the most powerful tool for quantitatively describing the evolution of local deformation [12–14]. Numerous full field methods are used for an experimental determination of fracture mechanics parameters related to cracks of detectable lengths [15–37]. Most of these techniques employ the measurements of in-plane displacement components related to cracks of constant length under step-by-step increase of external load. These fact means that a process of damage accumulation before a crack initiation cannot be quantitatively described. Moreover, measurement accuracy is not high enough for reliable involving derived parameters as representative damage indicators. Powerful numerical simulation techniques, which are based on refined description of elastic-plastic deformations near a crack tip, are used to overcome this problem [38–39].

The chief drawback of all above-mentioned approaches follows from the fact that a description of each discrete damage step employs parameters, which cannot reliably be established proceeding from direct physical measurements at different stages of low-cycle fatigue. The introduction of destructive methods is a powerful tool for obtaining highly accurate representative damage parameters. Previously, a destructive method was proposed with preliminary low-cycle fatigue loading of specimens with holes and applying a sequence of narrow notches at a constant external load. [40–42]. Singular and non-singular fracture mechanics parameters of artificial notches have been successfully involved as current damage indicators to quantify damage accumulation. Numerical integration of normalized evolution curves over lifetime provides the damage accumulation function in an explicit form. Employing the principles inherent in the non-destructive technique to create non-destructive methods of analyzing damage accumulation looks like a natural continuation of the developed methodology. This approach has been implemented for the quantitative analysis of low-cycle fatigue damage accumulation n the area of stress concentration as a result of the development of local deformation [43]. The key point, that defines scientific novelty and powerfulness of the developed approach, consists of involving various deformation parameters referred to critical point belonging to the open hole boundary as current damage indicators. It is of great importance that these parameters can be obtained for the single object. A capability of deriving damage indicator values corresponding to number of loading cycle related to arising surface macro-defect is the second remarkable feature of the proposed approach. Plane specimens with the centred open hole is undergone to low-cycle fatigue with stress range $\Delta\sigma$ = 350 MPa and stress ratio R = – 0.52 up to prefixed number of cycles, in the range from zero to 95% of the lifetime. Required strain values follow from distributions of all three displacement components along the hole edge measured by reflection hologram interferometry. The derived data at different stage of low-cycle fatigue lead to normalized dependencies of maximal strain value versus number of loading cycle, which are a source of the damage accumulation function.

Main subject of the present paper is to expand earlier developed novel non-destructive method for quantitative description of low-cycle fatigue damage accumulation in the stress concentration area to a case of contact interaction (the filled hole). The study of deformation kinetics of joint elements, especially under low-cycle fatigue conditions, is of both scientific and applied interest, in particular because of the large number of pins and rivets found in aircraft structures. The reliability of these separate pins or rivets exerts its main influence on the structure's lifetime [1–2]. There is a deficiency of reliable experimental data regarding the process of local elastic-plastic deformation in a plate containing a filled hole with a cylindrical inclusion as the model of individual pin or rivet joint element. That is why it is very difficult to formulate the effective approach for the prediction of a structure's lifetime based on quantitative damage accumulation analysis. We will try to illustrate one from possible ways to solve this problem.

EXPERIMENTAL PROCEDURE

Plane specimens of dimensions 260×60×6 mm, made from a hardening aluminium alloy of 2024 type, are used as the object of previous investigation [43]. The specimen has $2r_0$ =12 mm central open hole. The specimen was cut from 10 mm thick aluminium plate symmetrically in relation to its middle plane. Geometrical parameters of plane specimens, used in the present study, are completely analogous to the above-described specimens with the exception that the central hole is filled by the cylindrical pin with a push fit (no clearance or interference). The cylindrical steel pin was hardened to HRC = 42. Real fit parameters are the following: initial absolute clearance equals to Δd = 0.03 mm that corresponds to relative clearance $\delta d = 0.25\times10^{-2}$.

Drawing of the specimen, coordinate system and measured in-plane displacement components are shown in Fig. 1. Mechanical properties, obtained by standard tensile test, are the following: Young's modulus E = 74,000 MPa, yield stress σ_y = 330 MPa and Poisson's ratio μ = 0.33. Absence of technological residual stresses in the specimen follows from data of the probe hole drilling and further optical interferometric measurements of deformation response to local material removing [44]. The push-pull direction coincides with the rolling direction. A closed loop servo-hydraulic computer-aided testing machine MTS-250 was used to perform continuous fatigue loading program as well as step by step pseudo-static loading inside prescribed cycle automatically and accurately. The last circumstance is of decisive importance for reliable recording of high-quality reflection holographic interferograms at each individual loading step. This fact is essential for reliable deriving initial experimental information that has a form of displacement component distributions along the hole boundary.

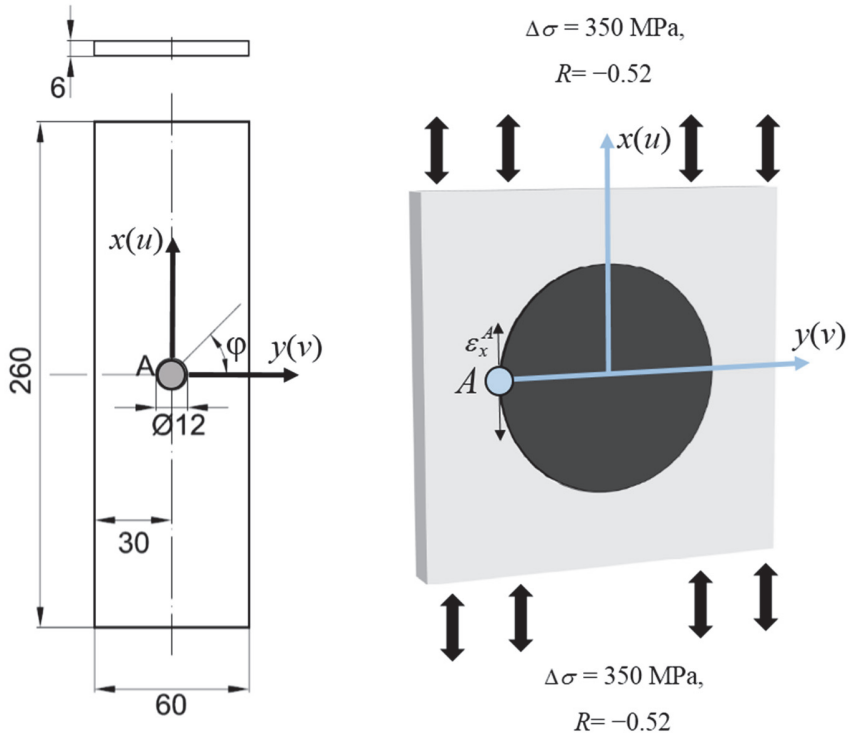

Figure 1: (a) Scheme of the specimen; (b) measurement parameters.

The experimental procedure for reflection holograms recording in opposite-beam arrangement and further reconstruction of interference fringe patterns is based on combining two-exposure and time-average technique to visualize the zero-order fringe. The detailed description of the technique involved for quantitative interpretation of interference fringe patterns to obtain the displacement components fields can be found in Ref. [14]. The developed experimental approach yields precision measurements of displacement component fields along the hole edge referred to all three Cartesian directions. This is achieved by introducing optimal interferometer system of the overlay interferometer in a combination with interpretation of obtained interference fringe patterns through the use of absolute fringe orders. The developed methodology maintains practical realization of the key merit inherent in reflection hologram interferometry. This advantage resides in a capability

of simultaneous determination of all three strain-induced displacement components with a measurement sensitivity is about of laser light wavelength (λ=0.6328 μm in the considered case). It is of importance that achieved measurement accuracy is high enough for reliable determination of local strains arising is stress concentration area.

Loading program has the following parameters: stress range $\Delta\sigma$ = 350 MPa; stress ratio R = –0.52; maximal remote stress σ_0^{MAX} = 230 MPa; minimal remote stress σ_0^{MIN} = –120 MPa. Remote stress is defined as current value of external force divided by specimen's cross-section. Thus, cyclic uniaxial tension compression is performed in the net stress range $-120 \le \sigma_0 \le 230$ MPa with a zero beginning point and a positive zero half cycle. The parameters of the loading cycle considered are those most typical for highly loaded components of pin/rivet joints of aircraft structures. Complete failure of the specimen with filled hole occurred after reaching 4160 cycles. This loading program completely coincides with the program used for the specimen with the open circular hole, for which fracture cycle number is equal to 1480 [43].

The choice of a fit type for quantitative damage accumulation analysis in the stress concentration zone in a presence of contact interaction has been raised by the following reasons. The results of the local deformation process investigation of the specimen with the open hole in the low-cycle range indicate fatigue crack appearance just before 1418th loading cycle. On the other hand, numerous data demonstrate that the hole filled by a pin with a relative interference parameter $\beta \ge 0.75\times10^{-2}$ leads to a considerable growth in the material resistance to fatigue damage accumulation [1–2, 14]. Therefore, push fit choice has been influenced by the need to maintain conditions of the contact interaction along a hole boundary, and at the same time to decrease the number of cycles before failure. The last circumstance is of importance to reduce the volume of technically complex and time-consuming experimental steps.

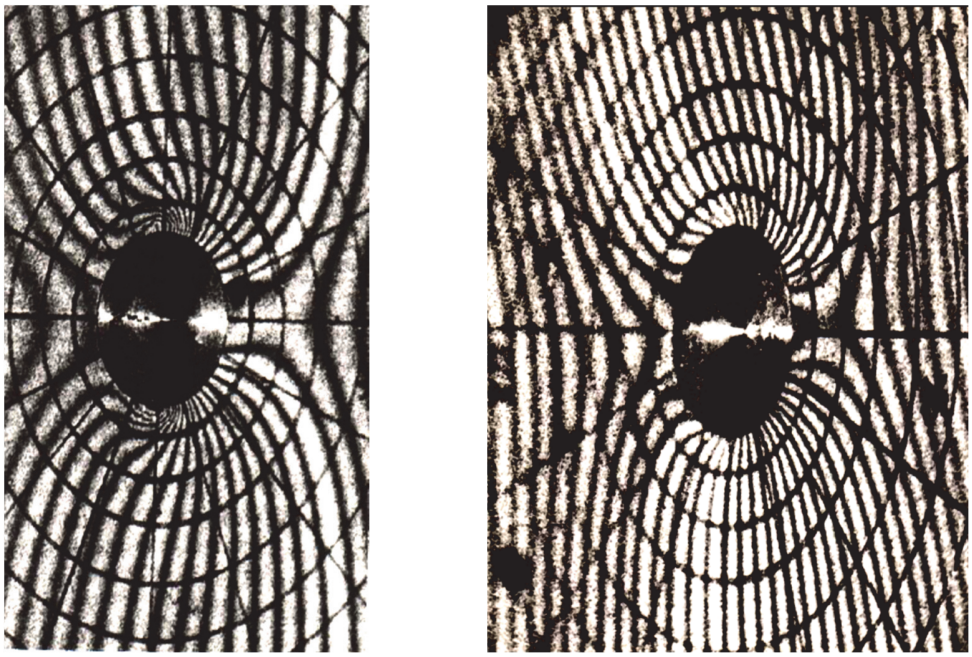

(a) (b)

Figure 2: Typical interferograms obtained at the first (a) and 1316th (b) loading cycle for practically equivalent remote stress increments.

Experimental technique includes the following main stages. The specimen is mounted into grips of universal servo-hydraulic testing machine. Holographic photo-plate is immediately clamped on the specimen surface area of interest by special glue in order to eliminate rigid body motions thus ensuring a reliable extraction of strain-induced in-plane displacement components to be measured. Quantitative description of local strain distributions around filled hole inherent in different stages of low-cycle fatigue is the main goal of this study. That is why step-by-step loading of the specimen together with sequential recording of reflection holographic interferograms have been performed to obtain the fringe pattern sets. These arrays of interferograms are essential to quantitatively describe a local deformation process at each prescribed loading cycle. This is attributed to the high sensitivity of holographic interferometry method. Quantitative characteristics of local deformation process have been obtained for the first, second, 14th, 115th, 735th, 1316th and 3530th loading cycles for the complete remote stress range, starting from zero to the maximum remote stress value σ_0^{MAX} = 230

MPa and then, through an intermediate zero point, to the minimum value σ_0^{MIN} = –120 MPa, and then again back to zero. Each loading step, at which specific reflection holographic interferogram is recorded, is defined by remote stress increment $\Delta\sigma_0^i = \sigma_0^{i+1} - \sigma_0^i$. In addition, the interferogram sets have been recorded on the 2900th, 3128th, 3931st, and 4133rd cycles for each zero to positive peak half cycle to obtain a detailed quantitative description of the fatigue crack initiation and further growth.

Typical interference fringe patterns obtained at the first (σ_0 from 135 to 162 MPa) and 1316th (σ_0 from 143 to 174 MPa) cycles at almost equivalent remote stress increments are shown in Fig. 2a and 2b, respectively. Horizontal and vertical diameters in Fig. 2 correspond to coordinate axis x and y shown in Fig. 1, respectively. It should be noted that interference fringes in these images do not have interruptions between the hole boundary and the lateral edges of the specimen.

Revealed fringe configuration evidences an absence of detectable defect of short crack type on the specimen surface. Such fringe behaviour is representative characteristic of the initial and stable stage of the local elastic-plastic deformation process. This means that accumulation of the material subsurface damages occurs during these stages only. The above-mentioned process exerts a very week influence on the material surface layers and cannot be discovered by means of holographic interferometry.

Typical distributions of the in-plane displacement components *u* (curves 1, 3) and *v* (curves 2, 4) in the Cartesian coordinate system along the line of contact interaction in the specimen with push fit (no clearance and interference between the hole boundary and the cylindrical steel inclusion) are presented in Fig. 3. These experimental dependencies correspond to the fringe patterns shown in Fig. 2.

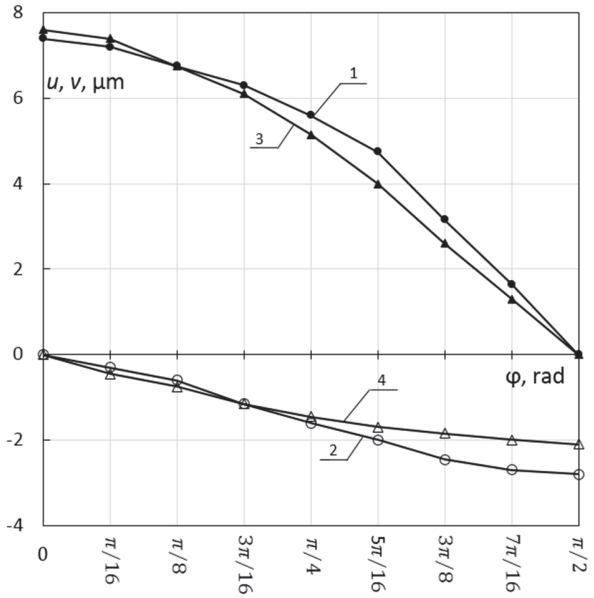

Figure 3: Distributions of in-plane displacement components (1, 3) an (2, 4) obtained at the 1st (remote stress increase from 135 to 162 MPa) and 1316th (remote stress increase from 143 to 174 MPa) loading cycle.

The distribution of the circumferential strain ε_φ along a circular hole boundary of r_0 radius, when the input data are expressed through displacement components *u* and *v* in the Cartesian coordinate system, has the following form:

$$\varepsilon_\varphi = \frac{1}{r_0}\left\{\frac{\partial v}{\partial \varphi}\cos\varphi - \frac{\partial u}{\partial \varphi}\sin\varphi\right\} \tag{1}$$

where polar angle φ is counted from tension-compression direction (*x*-axis) anti-clockwise (see Fig. 1a).

Numerical differentiation of discrete sets of initial experimental data, which is necessary for a determination of circumferential strain values according to formula (1), employs an approximation of displacement components *u* and *v* values by trigonometric series:

$$u = \sum_{k=1}^{p} A_k \cos k\varphi,\ v = \sum_{k=1}^{q} B_k \sin k\varphi\,, \tag{2}$$

where A_k and B_k follow from the least square method. Measurement uncertainty range sets a lower limit on A_k and B_k values from series (2), which are involved for strain calculation [8]:

$$A_k, B_k \geq \delta(u) = \delta(v) = 0.3\,\mu m \tag{3}$$

It should be noted that really measured in-plane displacement component values referred to all investigated cycles lie between 6 and 9 μm. Corresponding values of maximum tensile strain at the critical point A belonging to the hole edge ε_x^A fall in the range from 1.0×10^{-3} to 1.5×10^{-3}.

Fig. 4 demonstrates the circumferential strain distributions ε_φ along the hole boundary, relevant to Fig. 3.

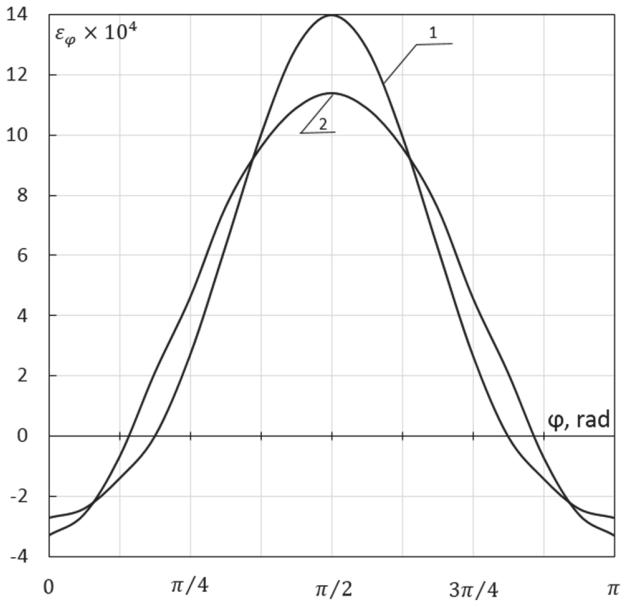

Figure 4: Distributions of the circumferential strains along the hole edge obtained at the first (1) and 1316th (2) loading cycles.

Holographic interferograms recorded during tension branch on the 2900th loading cycle clearly display an appearance of the surface damage. This damage has a form of short crack and is especially evident at the maximum remote stress level. To understand the influence of this factor on quantitative parameters of the local deformation process and damage accumulation, interferogram sets were recorded on the 2927th and 3530th loading cycles for the complete remote stress range ($-120 \leq \sigma_0 \leq 230$ MPa). Typical interferograms obtained on the 2927th and 3530th loading cycles for the same remote stress increment $\Delta\sigma_0$ from 135 to 162 MPa are shown in Fig. 5a and 5b, respectively. Horizontal and vertical diameters in Fig. 5 correspond to coordinate axis x and y shown in Fig. 1, respectively. Fringe interruptions can be reliably observed in this interference images near the point of maximum ε_φ values on the hole boundary This point is critical point A, which is located at the point of intersection of the hole boundary and vertical diameter in interference fringe patterns. Corresponding circumferential strain is denoted as ε_x^A. The values of the ε_x^A-strain are derived from formula (1) for $\varphi = \pi/2$ at each loading step. The interruptions are more clearly seen for the 3530th cycle. This fact gives a direct evidence of the short crack appearance on the specimen surface.

It is of interest to find a quantitative description of the phenomenon observed in terms of circumferential strains. Distributions of the tangential displacement component u (curve 1) and v (curve 2) in the Cartesian coordinate system along the hole boundary obtained on 2927th (circular dots) and 3530th (triangular dots) loading cycles are shown in Fig. 6. These graphs follow from interpretation of full interferogram sets, which include, in particular, images presented in Fig. 5.

Corresponding circumferential strain ε_φ distributions are shown in Fig. 7.

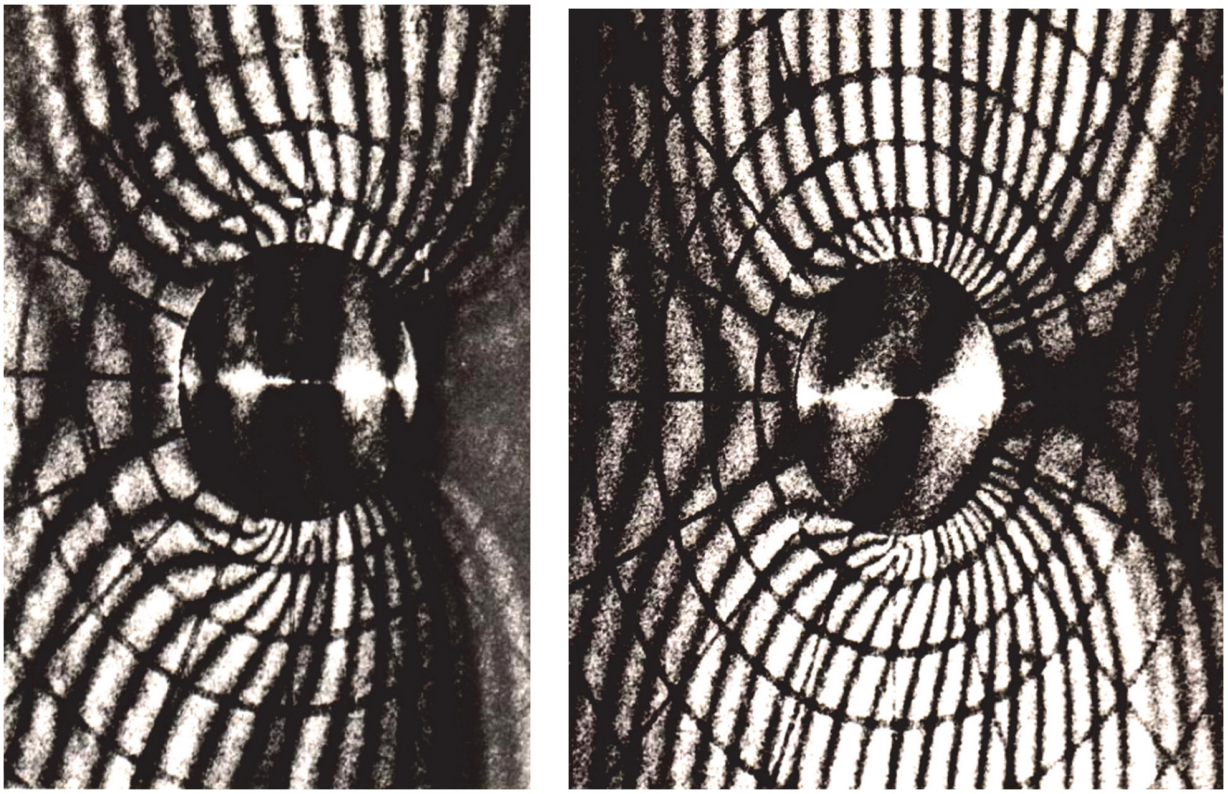

a b

Figure 5: Typical interferograms obtained at the same remote stress increments for the 2927th (a) and 3530th (b) loading cycles.

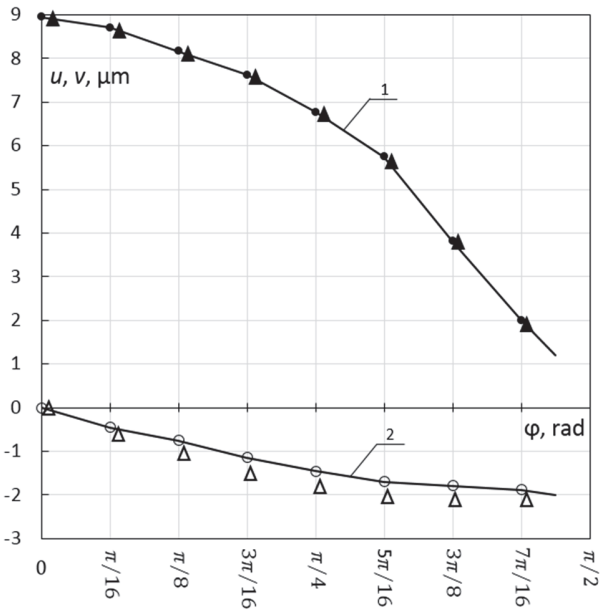

Figure 6: Distributions of the in-plane Cartesian displacement components u (1) and v (2) along the filled hole edge obtained after a surface crack appearance at 2927th (circular dots) and 3530th (triangular dots) loading cycles.

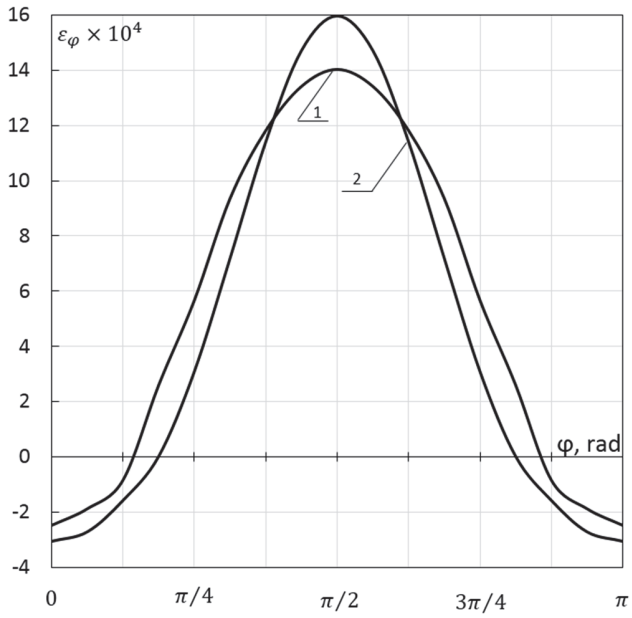

Figure 7: Distributions of the circumferential strains along the filled hole edge obtained after a surface crack appearance at 2927th (1) and 3530th (2) loading cycles.

It should be mentioned that plots presented in Fig. 6 do not reveal the considerable difference between corresponding displacement components for two loading cycles to be compared. Comparing two graphs in Fig. 7 demonstrates how relatively small differences in corresponding displacement components lead to a notable discrepancy in circumferential strain distributions.

The strain component ε_x can only be determined in contact interaction zone proceeding from the in-plane displacement component u and v derived through the use of reflection hologram interferometry data. It is possible to obtain a complete set of strain components, namely, ε_x, ε_y, ε_z and, hence, strain intensity ε_i at critical point $\boldsymbol{A}$, but for an open hole edge in plane rectangular specimen [14]. That is why only the component ε_x serves for constructing current damage indicators in the present study. This choice is not decisive. Damage accumulation functions, which are constructed for the specimen with the open hole proceeding from circumferential strain ε_φ and normal to the object surface strain ε_z, reveal very good coincidence [43].

EXTRACTING PARAMETERS

Practical realization of the involved non-destructive method for damage accumulation quantifying due to low-cycle fatigue needs an availability of reliable information concerning circumferential strain values at all investigated stages of low-cycle fatigue. Essential condition for reaching this goal resides in recording of high-quality reflection holographic interferograms at each loading step considered. This condition has been met in the course of the present study. Some typical interferograms, referred to different cycles and remote stress increments, are presented as illustrations in Fig. 2 and Fig. 5.

Whole set of distributions of circumferential strains along the filled hole edge, which are constructed for all loading steps inside of each loading cycles, allows extracting required parameters essential for quantitative damage accumulation analysis. Corresponding data arrays are listed in Tab. 1–4.

Data sets, which are analogous to information presented in Tab. 1–4, are also obtained for 14th, 735th, 1316th and 3530th loading cycles. Full volume of experimental data provides the dependencies of local strain at the point of maximum strain concentration (critical point A) ε_x^A as a function of remote stress level σ_0 for all considered cycles, which are shown in Fig. 8. Note that the distributions constructed for the 115th and 735th cycles practically coincide. Open and filled markers indicate the remote stress increasing and decreasing, respectively.

Stage number, k	Remote stress increment $\Delta\sigma_0^k$, MPa	Total remote stress value $\Sigma\Delta\sigma_0^k$, MPa	Maximum circumferential strain increment $\Delta\varepsilon_x^k \times 10^3$	Total maximum circumferential strain value $\Sigma\Delta\varepsilon_x^k \times 10^3$
1	35.0	35.0	1.26	1.26
2	35.0	70.0	1.30	2.56
3	35.0	105.0	1.26	3.82
4	30.0	135.0	1.23	5.05
5	27.0	162.0	1.39	6.44
6	25.0	187.0	1.81	8.25
7	23.0	210.0	1.65	9.90
8	**20.0**	**230.0**	2.00	**11.90 = ε_x^{A-MAX}**
9	–30.0	200.0	–1.04	10.86
10	–30.0	170.0	–1.22	9.64
11	–35.0	135.0	–1.38	8.26
12	–35.0	100.0	–1.23	7.03
13	–35.0	65.0	–1.33	5.70
14	–35.0	30.0	–1.36	4.44
15	–30.0	0.0	–1.23	3.21
16	–30.0	–30.0	–1.27	1.94
17	–30.0	–60.0	–1.08	0.86
18	–30.0	–90.0	–1.33	–0.47
19	–30.0	**–120.0**	–0.98	**–1.45 = ε_x^{A-MIN}**
20	30.0	–90.0	0.63	–0.82
21	30.0	–60.0	0.63	–0.19
22	30.0	–30.0	0.81	0.70

Table 1: Load stages and results of fringe patterns interpretation for the first cycle.

Stage number, k	Remote stress increment $\Delta\sigma_0^k$, MPa	Total remote stress value $\Sigma\Delta\sigma_0^k$, MPa	Maximum circumferential strain increment $\Delta\varepsilon_x^k \times 10^3$	Total maximum circumferential strain value $\Sigma\Delta\varepsilon_x^k \times 10^3$
1	35.0	35.0	1.41	1.41
2	38.0	73.0	1.49	2.90
3	38.0	111.0	1.55	4.45
4	35.0	146.0	1.40	5.85
5	30.0	176.0	1.23	7.08
6	28.0	204.0	1.24	8.32
7	26.0	**230.0**	1.22	**9.54 = ε_x^{A-MAX}**
8	–37.0	193.0	–1.25	8.29
9	–38.0	155.0	–1.44	6.85
10	–37.0	118.0	–1.47	5.38
11	–38.0	80.0	–1.36	4.02
12	–38.0	42.0	–1.40	2.62
13	–37.0	5.0	–1.43	1.19
14	–35.0	–30.0	–1.37	–0.18
15	–30.0	–60.0	–0.94	–1.12
16	–30.0	–90.0	–0.90	–2.02
17	–30.0	**–120.0**	–0.85	**–2.87 = ε_x^{A-MIN}**
18	30.0	–90.0	0.80	–2.07
19	30.0	–60.0	0.81	–1.26
20	30.0	–30.0	0.83	–0.43
21	30.0	0.0	0.73	0.40

Table 2: Load stages and results of fringe patterns interpretation for the second cycle.

Stage number, k	Remote stress increment $\Delta\sigma_0^k$, MPa	Total remote stress value $\Sigma\Delta\sigma_0^k$, MPa	Maximum circumferential strain increment $\Delta\varepsilon_x^k \times 10^3$	Total maximum circumferential strain value $\Sigma\Delta\varepsilon_x^k \times 10^3$
1	35.0	35.0	1.50	1.50
2	37.0	72.0	1.55	3.05
3	37.0	109.0	1.56	4.61
4	34.0	143.0	1.34	5.95
5	31.0	174.0	1.25	7.20
6	29.0	203.0	1.15	8.35
7	27.0	**230.0**	1.13	**9.48 = ε_x^{A-MAX}**
8	–37.0	193.0	–1.44	8.02
9	–38.0	155.0	–1.38	6.64
10	–37.0	118.0	–1.44	5.15
11	–38.0	80.0	–1.51	3.64
12	–38.0	42.0	–1.50	2.14
13	–37.0	5.0	–1.50	0.64
14	–35.0	–30.0	–1.40	–0.76
15	–30.0	–60.0	–0.94	–1.70
16	–30.0	–90.0	–0.90	–2.60
17	–30.0	**–120.0**	–0.90	**–3.50 = ε_x^{A-MIN}**
18	30.0	–90.0	0.80	–2.70
19	30.0	–60.0	0.82	–1.88
20	30.0	–30.0	0.88	–1.00
21	30.0	0.0	1.25	0.25

Table 3: Load stages and results of fringe patterns interpretation for the 115th cycle.

Stage number, k	Remote stress increment $\Delta\sigma_0^k$, MPa	Total remote stress value $\Sigma\Delta\sigma_0^k$, MPa	Maximum circumferential strain increment $\Delta\varepsilon_x^k \times 10^3$	Total maximum circumferential strain value $\Sigma\Delta\varepsilon_x^k \times 10^3$
1	40.0	40.0	1.67	1.67
2	40.0	80.0	1.63	3.30
3	40.0	120.0	1.53	4.83
4	40.0	160.0	1.54	6.37
5	35.0	195.0	1.41	7.78
6	35.0	**230.0**	1.44	**9.22 = ε_x^{A-MAX}**
7	35.0	195.0	–1.28	7.94
8	35.0	160.0	–1.41	6.53
9	40.0	120.0	–1.65	4.88
10	40.0	80.0	–1.65	3.23
11	40.0	40.0	–1.57	1.66
12	40.0	0.0	–1.57	0.09
13	–40.0	–40.0	–1.45	–1.36
14	–40.0	–80.0	–1.16	–2.52
15	–40.0	**–120.0**	–1.10	**–3.62 = ε_x^{A-MIN}**
16	40.0	–80.0	1.14	–2.48
17	40.0	–40.0	1.24	–1.24
18	40.0	–0.0	1.46	0.22

Table 4: Load stages and results of fringe patterns interpretation for the 2927th cycle.

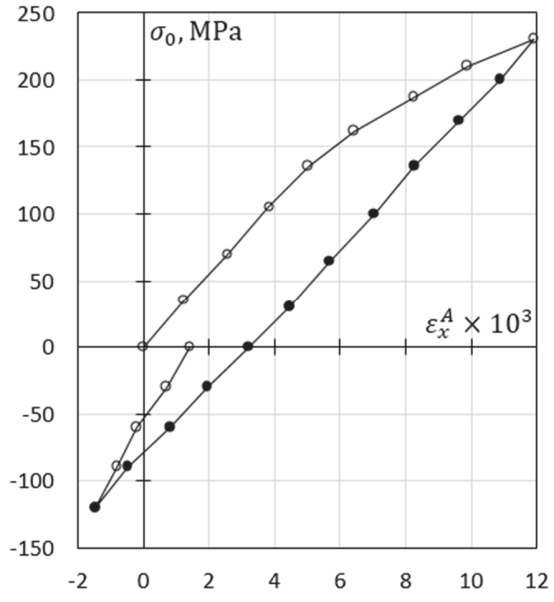
σ_0, MPa
$\varepsilon_x^A \times 10^3$
250
200
150
100
50
0
-50
-100
-150
-2
0
2
4
6
8
10
12

a

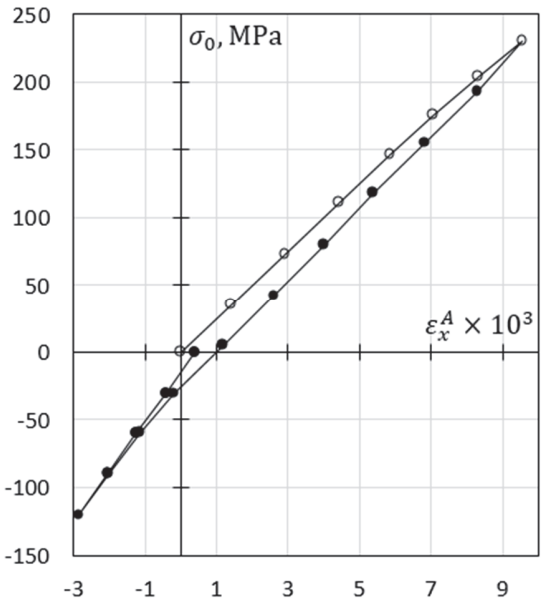
σ_0, MPa
$\varepsilon_x^A \times 10^3$
250
200
150
100
50
0
-50
-100
-150
-3
-1
1
3
5
7
9

b

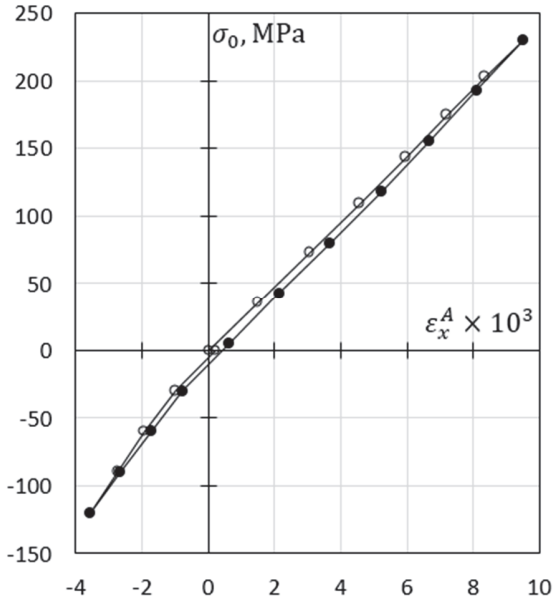
σ_0, MPa
$\varepsilon_x^A \times 10^3$
250
200
150
100
50
0
-50
-100
-150
-4
-2
0
2
4
6
8
10

c

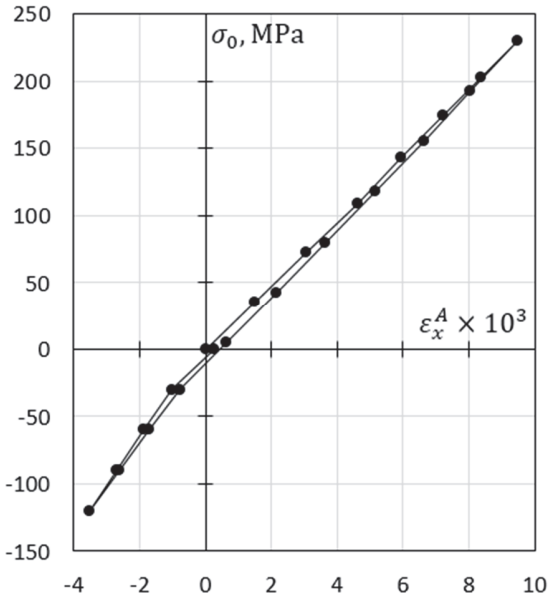
σ_0, MPa
$\varepsilon_x^A \times 10^3$
250
200
150
100
50
0
-50
-100
-150
-4
-2
0
2
4
6
8
10

d

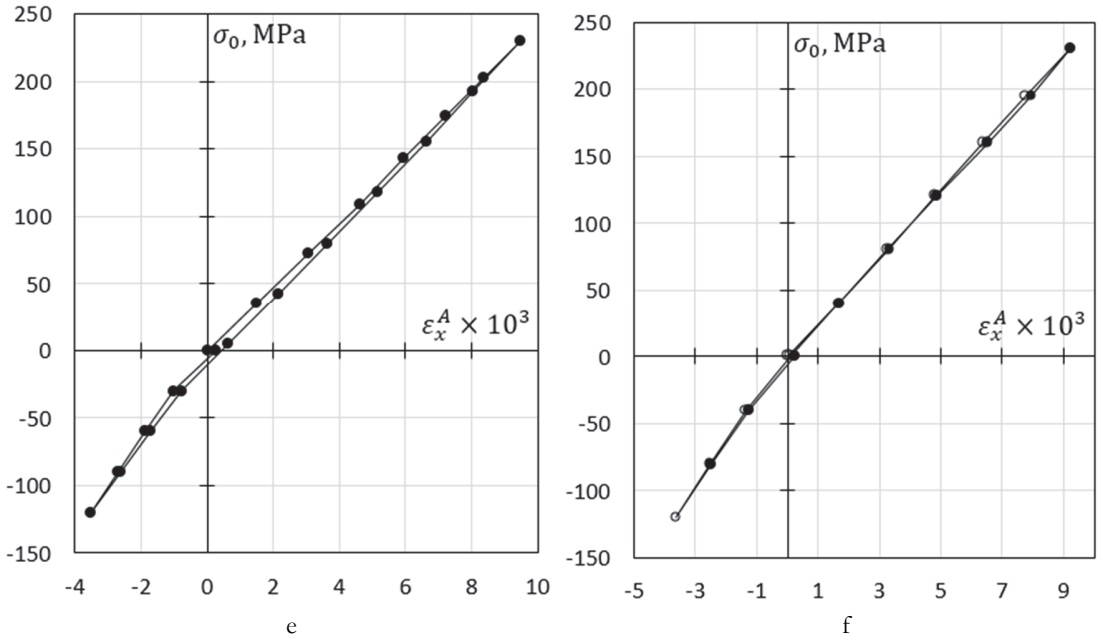

Figure 8: Dependencies of maximum circumferential strain at the hole edge versus remote stress level for the following cycles of loading: the first (a), the second (b), 14th (c), 115th (d), 1316th (e), 2927th (f), and 3530th (g) loading cycles.

Cicles number, N	1	2	14	115	735	1316	2927	3530
$\ln N$	0	0.69	2.64	4.75	6.60	7.18	8.00	8.17
$\varepsilon_x^{A-MAX} \times 10^3$	11.90	9.54	9.52	9.48	9.10	8.68	9.22	10.65
$\varepsilon_x^{A-MIN} \times 10^3$	–1.45	–2.87	–3.56	–3.50	–3.80	–4.15	–3.62	–3.81
$\Delta\varepsilon_x^A \times 10^3$	13.35	12.41	13.08	12.98	12.90	12.83	12.84	14.46

Table 5: Local deformation parameters, obtained at different stages of low-cycle fatigue: ε_x^{A-MAX} is maximal local strain; ε_x^{A-MIN} is minimal local strain; $\Delta\varepsilon_x^A$ is strain range referred to the critical point ***A*** at the boundary of the filled hole.

Tab. 5 and Fig. 9 include data, describing an evolution of local deformation parameters up to short crack appearance, which are essential for further deriving of current damage indicators.

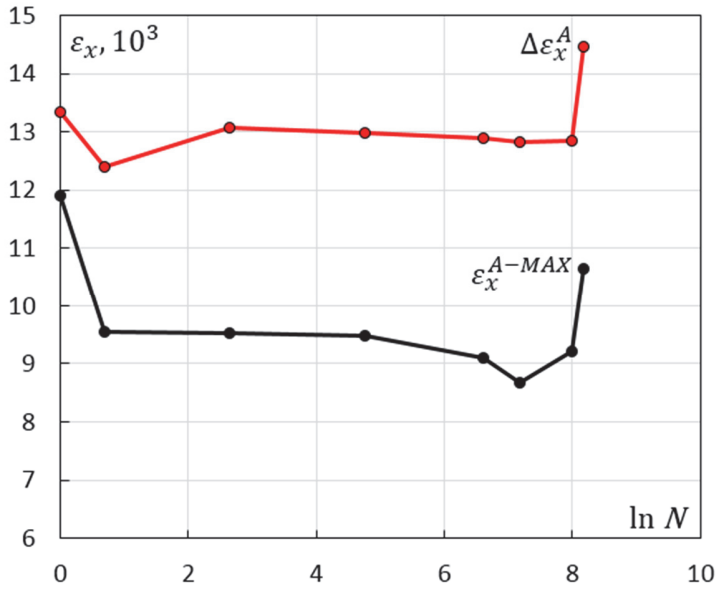

Figure 9: Maximal local strain ε_x^{A-MAX} and local strain range $\Delta\varepsilon_x$ as a function of loading cycle number N referred to critical point at the filled hole edge.

THEORETICAL BACKGROUND AND DAMAGE ACCUMULATION FUNCTION

A monotonically varying parameter must be introduced into consideration to ultimately obtain a quantitative description of fatigue damage accumulation [3]. Number of loading cycles N_m is precisely this parameter in the involved problem. Each damage indicator, when stress range and stress ratio are definitely given, depends on number of cycles N_m and chosen physical value that is measured at different stage of low-cycle fatigue. That is why, there is a good reason to introduce into consideration the damage accumulation function $D_m\left(N_m,\varepsilon(k)\right)$, which characterizes current damage degree proceeding from an evolution of deformation parameters referred to the hole edge. Variation of this function during low-cycle fatigue is subjected to kinetic equation [3]:

$$\frac{dD_m\left(N_m,\varepsilon(k)\right)}{dN_m}=\Psi^k\left(N_m,\varepsilon(k)\right), \tag{4}$$

where $\Psi^k\left(N_m,\varepsilon(k)\right)$ is the damage accumulation rate; $\varepsilon(k)$ defines fracture mechanics parameter used for the analysis: $\varepsilon(1)$ is strain range referred to critical point A at the hole edge $\Delta\varepsilon_x^A$; $\varepsilon(2)$ is maximal tensile strain referred to critical point A at the hole edge ε_x^{A-MAX}. The damage accumulation function can be derived by integration of Eqn. (1):

$$dD_m\left(N_m,\varepsilon(k)\right)=\int_0^{N_F^G}\Psi^k(N_m,\varepsilon(k))dN_m\,. \tag{5}$$

Boundary conditions inherent in the damage accumulation function $dD_m\left(N_m,\varepsilon(k)\right)$ must obey the following equations:

$$D_m\left(N_m=0,\varepsilon(k)\right)=0\,,\quad D_m\left(N_m=N_F^{Cr},\varepsilon(k)\right)=1\,. \tag{6}$$

The second limiting case $D_m=1$ in relationships (6) is related to $N_m=N_F^{Cr}$ that corresponds to short crack appearance at the external specimen face. A capability to reveal loading cycle number that corresponds to surface macro-defect arising and obtaining required value of chosen deformation parameter is a remarkable feature of the proposed non-destructive approach. This is evident advantage over the destructive technique based on the narrow notch inserting and further fracture mechanics parameters determination, which involves complete separations of the specimen by two fragments as the second limit case [40–42, 45].

An explicit form of the function $\Psi^k\left(N_m,\varepsilon(k)\right)$ from Eqns. (4) and (5) can be presented as:

$$\Psi^k\left(N_m,\varepsilon(k)\right)=\frac{S_D^k(k)\times\varepsilon(k,N_m)}{\varepsilon(k,N_m=0)\times N_F^{Cr}} \tag{7}$$

where N_m is current number of loading cycle; $S_D^k(k)$ is normalizing coefficient that must be derived from the experimental data for each specific damage indicator; $\varepsilon(k,N_m)$ is a set of experimental values of damage indicator, obtained after reaching N_m cycles; $\varepsilon(k,N_m=0)$ is a value of chosen damage indicator that corresponds to maximum level of tensile remote stress for the first half cycle; $N_m=N_F^{Cr}$ means loading cycle number that corresponds to short crack appearance at the external specimen face.

Substitution of the function $\Psi^k\left(N_m,\varepsilon(k)\right)$ from Eqn. (7) into relationship (5) and summarizing along the segments $\Delta N_m=N_{m+1}-N_m$, at end points of which values of chosen damage indicator $\varepsilon(k,N_m)$ have been determined instead of integration, gives the explicit form of the damage accumulation function:

$$D_m\left(N_m,\varepsilon(k)\right)=\sum_{N_m=0}^{N_m=N_F^{Cr}}\frac{S_D^k(k)\times\varepsilon(k,N_m)}{\varepsilon(k,N_m=0)\times N_F^{Cr}\times\Delta N_m} \tag{8}$$

where $\Delta N_m=N_{m+1}-N_m$ denotes number of loading cycles between two neighbouring points of $\varepsilon(k,N_m)$ determination.

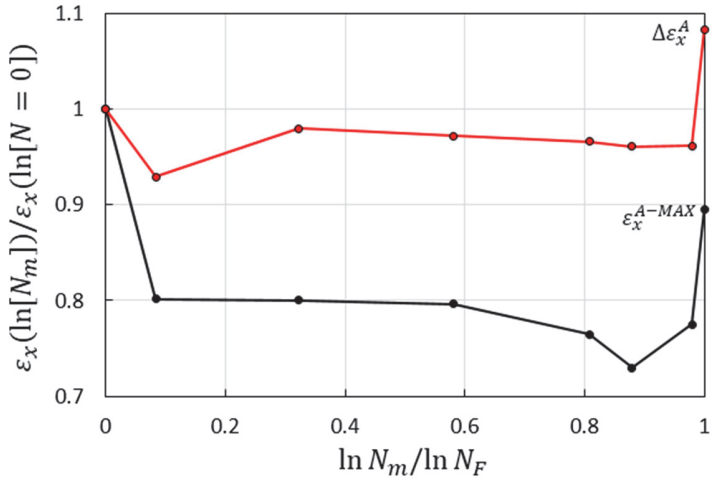

Figure 10: Evolution of normalized deformation parameters $\varepsilon(1)=\Delta\varepsilon_x^A$ and $\varepsilon(2)=\varepsilon_x^{A-MAX}$ in the range from $N_m=0$ to $N_m=N_F^{Cr}$.

The coefficient $S_D^k(k)$ for specimens of given geometrical dimensions is defined by mechanical properties material and parameters of loading program. The value of the coefficient $S_D^k(R_i)$ in each specific case follows from normalization of Eqn. (8) taking into account that the total sum in the right-hand side must be equal to one. This is attributed to the definition of limiting values of the damage accumulation function (6). The required procedure is based on the use of normalized distribution of each damage indicator $\varepsilon(k, N_m)$ as a function of loading cycle number, which are constructed in the range from $N_m = 0$ to $N_m = N_F^{Cr}$. These dependencies are presented in Fig. 10.

A square lying under each normalized $\varepsilon(1)$ curve, shown in Fig. 10, represents by itself initial experimental information essential for a calculation of the coefficient $S_D^k(k)$. This square is denoted as $\Sigma\varepsilon(k)$. Required coefficients are derived as an inverse proportional values:

$$S_D^k(k) = 1/\Sigma\varepsilon(k). \tag{9}$$

The developed procedure leads to an explicit form of the damage accumulation function (8). Data presented in Fig. 10 and Formula (9) provide normalizing coefficient values, which are listed in Tab. 6.

Damage indicator, $\varepsilon(k)$	Square under normalized curve $\Sigma\varepsilon(k)$, conventional units	Normalizing coefficient $S_D^k(k)$
$\varepsilon(1)$	0.967	1.03
$\varepsilon(2)$	0.796	1.26

Table 6: Values of normalizing coefficients $S_D^k(k)$.

Graphical representation of Formula (8) implementation by using Tab. 5 data for obtaining an explicit form of the damage accumulation function are shown in Fig. 11.

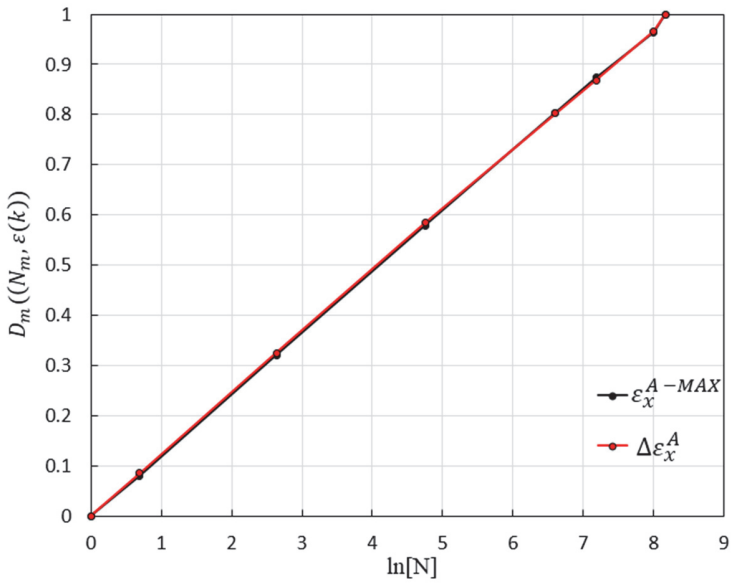

Figure 11: The damage accumulation function $D_m(N_m, \varepsilon(k))$ constructed proceeding from the evolution of different damage indicators.

Plots presented in Fig. 11 clearly evidence practically coinciding damage accumulation functions, which follow from two different damage indicators. This fact, firstly, demonstrate highly accurate character of the measurement procedure based on reflection hologram interferometry. Second, revealed coincidence confirms a high representative level of both damage indicators involved. This fact is also of importance from the experimental standpoint. The matter is that obtaining complete set of interference fringe patterns, which are essential for a determination of maximum strain range $\Delta\varepsilon_x^A$, demands recording and reconstruction of 18–22 reflection holograms as it follows from Tab. 1–4. The same data show that obtaining reduced interferogram set for ε_x^{A-MAX} determination needs an availability of 6–8 reflection holograms.

The damage accumulation function has been earlier obtained for geometrically analogous specimen with the open hole under the same cycle parameters [43]. This circumstance provides a way for direct comparison of two cases considered. Fig. 12 clearly illustrates how a contact interaction decreases the damage accumulation rate.

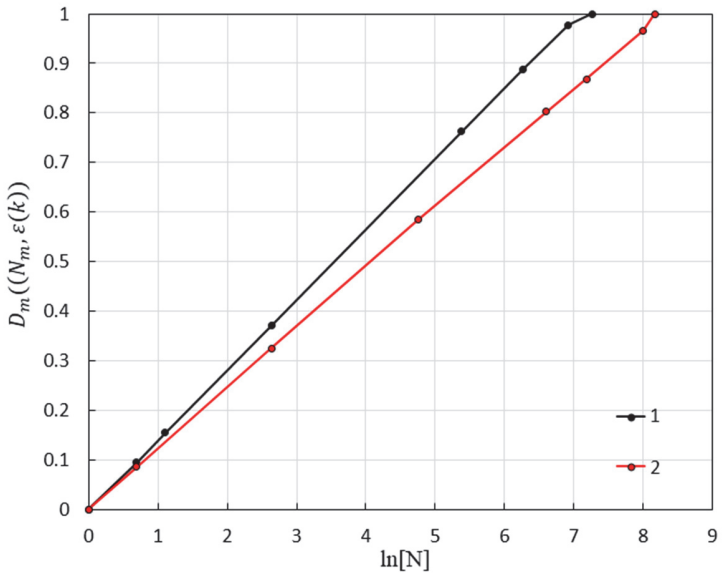

Figure 11: Damage accumulation functions obtained for geometrically analogous specimens with open (1) and filled (2) holes for the same low-cycle fatigue conditions.

Discussion

A sequence of research steps, which are essential for creating unconventional non-destructive method of damage accumulation quantifying under low-cycle fatigue conditions, has been arranged and successfully performed. These steps follow from regular trends provided by an experience of destructive technique implementation. Remarkable capability of quantitative description of damage accumulation proceeding from the evolution of fracture mechanics parameters has earlier been proposed and substantiated. Involved values of both singular (the stress intensity factor, SIF) and non-singular (in-plane displacement components, the T-stress) fracture mechanics parameters are relevant to the artificial narrow notch, which is emanated from the boundary of the open hole and is inserted under constant external load at different stages of low-cycle fatigue. The developed approach employs periodic pull-push loading of specimens of equal geometrical configuration up to prefixed cycle number thus reaching different damage level for each specific specimen. Deformation response to local material removing is measured by electronic speckle pattern interferometry in terms of in-plane displacement components. Inserted notches manifest a fatigue damage accumulation level similar to the probe hole for residual stress energy release in the hole-drilling method.

Transfer from destructive to non-destructive technique demands one essential procedure. Namely, it must be reliably established whether the deformation characteristics related to the stress concentration region can be used as representative indicators of damage. First step in this direction resides in involving non-singular fracture mechanics parameters, namely, in-plane displacement components referred to notch borders, in the process of quantifying damage accumulation under low-cycle fatigue. The conducted research give a positive answer to this question both for a plain [42] and for an open hole with cold expansion. The in-plane displacement components measured near the crack tip, as well as the resulting SIF and

T-stress values, serve as indicators of current damage. Numerical integration of the normalized dependences describing the evolution over the entire service life of both non-singular (in-plane displacement components, T-stress) and singular (SIF) parameters gives an explicit form of damage accumulation functions. It has been established that damage accumulation functions provided by different damage indicators practically coincide for each specific specimen subjected to low-cycle fatigue with fixed stress ratio and stress range. Thus, we have obtained a good reason to believe that deformation characteristics related to the hole edge can be reliably introduced as current damage indicators, including a contact interaction case. Distinctive future of the proposed approach consists of the fact that required deformations can be extracted without inserting the narrow notch.

The following essential achievements have been reached in the framework of the presented research in order to develop the novel non-destructive method of quantitative analysis of damage accumulation caused by low-cycle fatigue in the stress concentration zone in a case of contact interaction:

– The main scientific novelty of the proposed approach resides in involving directly measured deformation characteristics as current damage indicators. These indicators are maximal circumferential strain range and maximal circumferential strain values. All parameters are relevant to the critical point belonging to the hole edge and are derived without inserting the narrow notch. This crucial fact means that the damage accumulation function can be constructed by using single specimen for given stress range and stress ratio. Previously, the developed destructive method needs 8-10 specimens of the same dimensions to reach the above-mentioned goal. A capability of considering an instant of short crack appearance on the object surface as the limit case in the course of obtaining the explicit form of the damage accumulation function is the second peculiarity. Third advantage of the non-destructive method resides in its applicability to the contact interaction case. Naturally, inserting the artificial notch is impossible when a hole is filled by the cylindrical inclusion.

– The mathematical substantiation necessary for the implementation of a new non-destructive method for the quantitative description of the accumulation of low-cycle fatigue damage is given. It is shown that normalized values of deformation parameters, which are experimentally obtained for the critical point located at the filled hole edge at different stages of low-cycle fatigue, can reliably be used as current damage indicator. Thus, numerical integration of evolution curves over chosen cycle range produces the damage accumulation function within a normalizing coefficient. The required coefficient is derived as an inverse proportional value with respect to a square lying under the normalized evolution curve. The developed procedure defines the explicit form of the damage accumulation function for each specific deformation-based damage indicator.

– Practical implementation and verification of the non-destructive approach is performed by investigation of local deformation process inherent in the boundary of the filled hole in plane rectangular specimens measuring 260×60×6 mm under periodical uniaxial push-pull loading with stress range 350 MPa and stress ratio 0.52. Deformation characteristics are obtained for 1, 2, 14, 115, 1316, 2927, 3530 cycles. Normalized dependencies of current damage indicators against number of loading cycles are constructed from these data.

– Derived information provides the explicit form of damage accumulation functions on a base of developed theoretical foundations. These functions are obtained from two damage indicators. It is established that all involved damage indicators lead to practically coinciding results. This fact is reliable corroboration of high representative level inherent in two considered damage indicators for the filled hole in the case of contact interaction. Comparing data, obtained for two different specimens, quantitatively describe a contact interaction influence on the damage accumulation rate.

Like all experimental approaches, destructive and non-destructive methods related to the study of fatigue damage accumulation have characteristic disadvantages and advantages. There is no way to implement destructive research tools for real engineering components. Most obvious advantage of the destructive approach resides in highly accurate determination of representative damage indicators in terms of fracture mechanics parameters proceeding from relatively simple experimental procedure. The trouble with the destructive method is that it needs 8-10 specimens of the same dimensions, which are accurately produced by the same technology, to obtain the damage accumulation function for given parameters of low-cycle fatigue.

The developed non-destructive method allows constructing the damage accumulation function by using single specimen for given stress range and stress ratio. Using an instant of short crack appearance on the object surface as the limit case for obtaining the explicit form of the damage accumulation function is second peculiarity. Third advantage of the non-destructive method resides in its applicability to the contact interaction case. A complexity of the experimental technique, which is based on reflection hologram interferometry, is the single pronounced disadvantage of the developed technique. What is the level of this complexity compared to other known non-destructive methods for quantitative analysis of damage accumulation?

A promising step in a way to quantify damage is to use the evolution of surface roughness to predict the crack initiation. [46]. But, relatively simple implementation of this technique is retarded by difficulties related to reliable identification of surface roughness parameters which can represent damage accumulation in the material.
An excellent example of the study directed toward establishing physical essence of the fatigue crack initiation through the use of non-destructive methods is presented in Ref. [47]: «A new combined experimental and modelling approach has been developed in order to understand the physical mechanisms that lead to crack nucleation in a polycrystalline aluminium alloy AA2024 undergoing cyclic loading. Four-point bending low-cycle fatigue tests were performed inside the chamber of a scanning electron microscope on specimens with through-thickness central hole, introduced to localize stresses and strains in a small region on the top surface of the sample. Fatigue crack initiation and small crack growth mechanisms were analyzed through high-resolution scanning electron microscope images, local orientation measurements using electron-back-scattered-diffraction, and local strain measurements using digital image correlation». Thus, a tremendous arsenal of ultra-modern and high-expensive research tools has been perfectly implemented for quantifying damage accumulation. It is clear that the experimental complexity of the technique based on high-resolution scanning electron microscopy far exceeds the technical problems associated with reflective hologram interferometry.

Conclusions

The novel non-destructive method for quantitative description of low-cycle fatigue damage accumulation is expanded to a case of contact interaction in the stress concentration area. The key point, that defines scientific novelty and powerfulness of the developed approach, consists of involving local deformation parameters, measured by reflection hologram interferometry, as current damage indicators. The data, which are derived at different stages of low-cycle fatigue for the single specimen, provide normalized dependencies of local strain values versus number of loading cycle. This information is a source of damage accumulation functions. These functions are constructed for the specimen with the filled hole and geometrically analogous specimen with the open hole. The obtained data quantitatively describe a difference in damage accumulation rates for two cases.

Acknowledgements

The authors acknowledge the support of the Russian Science Foundation (project N 18-19-00351).

References

[1] Osgood, C.C. (1982). Fatigue Design. Pergamon Press, Oxford.
[2] Collins, J. A. (1993). Failure of Materials in Mechanical Design: Analysis, Prediction, Prevention, 2nd edition. NY, Chichester, Brisbane, Toronto, Singapure: John Wiley & Sons, 672.
[3] Murakami, S. (2012). Continuum Damage Mechanics. Springer Dordrecht Heidelberg London New York, 402. DOI: 10.1007/978-94-007-2666-6.
[4] Makhutov, N., Matvienko, Yu., Chernyakov, S. (1993). A unified methodological approach to calculation analysis of the stages of nucleation and growth of low-cycle fatigue cracks, Materials Science, 29, pp. 109–114.
[5] Zerbst, U., Klinger, C., Clegg, R. (2015). Fracture mechanics as a tool in failure analysis – prospects and limitations, Engineering Failure Analysis, 55, pp. 376-410. DOI: 10.1016/j.engfailanal.2015.07.001.
[6] Shahani, A.R., Mohammadi, S. (2015). Damage tolerance approach for analyzing a helicopter main rotor blade, Engineering Failure Analysis, 57, pp. 56-71, DOI: 10.1016/j.engfailanal.2015.07.02
[7] Correia, J.A.F.O., Balsón, S., De Jesus, A.M.P., Canteli, A.F., Moreira, P.M.G.P., Tavares, P. J. (2016). Fatigue life prediction based on an equivalent initial flaw size approach and a new normalized fatigue crack growth model, Engineering Failure Analysis, 69, pp. 15-28. DOI: 10.1016/j.engfailanal.2016.04.003.
[8] Marques, F., Correia, J.A.F.O., Abílio de Jesus, M.P., Cunha, Á., Caetano, E., Fernandes, A.A. (2018). Fatigue analysis of a railway bridge based on fracture mechanics and local modelling of riveted connections, Engineering Failure Analysis, 94, pp. 121–144. DOI: 10.1016/j.engfailanal.2018.07.016.

[9] Goyal, R., Bogdanov, S., El-zein, M., Glinka, G. (2018). Fracture mechanics based estimation of fatigue lives of laser welded joints, Engineering Failure Analysis, 93, pp. 340–355. DOI: 10.1016/j.engfailanal.2018.07.017.
[10] Szusta, A., Seweryn, A. (2015). Damage accumulation modeling under uniaxial low cycle fatigue at elevated temperatures, Engineering Failure Analysis, 56, pp. 474-483.
[11] Farahani, B. V., Belinha, J., Amaral, R., Tavares, P. J., & Moreira, P. (2018). A digital image correlation analysis on a sheet AA6061-T6 bi-failure specimen to predict static failure. Engineering Failure Analysis, 90, pp. 179–196. DOI:10.1016/j.engfailanal.2018.03.
[12] Chiang, F.-P. (1993). Moiré and speckle methods applied to elastic-plastic fracture studies, In: Experimental Techniques in Fracture mechanics, 3rd edition, Edited by J.S. Epstein. NY: VCH, pp. 291 – 325.
[13] Post, D., Han, B., Ifju, P. (1994). High Sensitivity Moiré, Exp. Analysis for Mech. and Mat. Berlin: Springer Verlag, p. 444.
[14] Shchepinov, V.P., Pisarev, V.S., Novikov, S.A., Balalov, V.V., Odintsev, I.N., Bondarenko, M.M. (1996). Strain and Stress Analysis by Holographic and Speckle Interferometry, Chichester: John Wiley, p. 483.
[15] Lee, C., Chao, Y.J., Sutton, M.A., Peters, W.H., Ranson, W.F. (1989). Determination of plastic strains at notches by image-processing methods, Exp. Mech., 29, pp. 214–220.
[16] Steckenrider, J., Wagner, J. (1995). Computed speckle decorrelation (CSD) for the study of fatigue damage, Optics & lasers in Engineering, 22, pp. 3–15.
[17] Diaz, E.V., Kaufmann, G.H., Armas, A.E., Galizzi, G.E. (2001). Optical measurement of the plastic zone size in a notched metal specimen subjected to low-cycle fatigue, Optics & lasers in Engineering, 35, pp. 325–333.
[18] Diaz, E.V., Armas, A.E., Kaufmann, G.H., Galizzi, G.E. (2004). Fatigue damage accumulation around a notch using a digital image measurement system, Experimental Mechanics, 44, pp. 241–246.
[19] López-Crespo, P., Burguete, R. L., Patterson, E. A., Shterenlikht, A., Withers, P. J., & Yates, J. R. (2008). Study of a Crack at a Fastener Hole by Digital Image Correlation, Experimental Mechanics, 49(4), 551–559. DOI:10.1007/s11340-008-9161-1
[20] Hamam, R., Hild, F., Roux, S. (2007). Stress intensity factor gauging by digital image correlation: Application in cyclic fatigue, Strain, 43, pp. 81-192.
[21] Yates, J.R. et al. (2008). Crack paths under mixed mode loading, Eng. Fract. Mech, 75, pp. 319-330.
[22] Yates, J.R., Zanganeh, M., Tomlinson, R.A., Brown, M.W., & Garrido, F.A.D. (2008). Crack paths under mixed mode loading, Engineering Fracture Mechanics, 75(3-4), pp. 319-330. doi:10.1016/j.engfracmech.2007.05.014 10.1016
[23] Backman, D., Liao, M., Crichlow, L., Yanishevsky, M., & Patterson, E. A. (2008). The use of digital image correlation in a parametric study on the effect of edge distance and thickness on residual strains after hole cold expansion, The Journal of Strain Analysis for Engineering Design, 43(8), pp. 781–789. DOI:10.1243/03093247jsa448
[24] Lopez-Crespo, P., Shterenlikht, A., Patterson, E. A., Yates, J. R., & Withers, P. J. (2008). The stress intensity of mixed mode cracks determined by digital image correlation, The Journal of Strain Analysis for Engineering Design, 43(8), pp. 769–780. DOI:10.1243/03093247jsa419
[25] López-Crespo, P. et al. (2009). Study of a crack at a fastener hole by digital image correlation, Experimental Mechanics, 49, pp. 551–559. DOI: 10.1007/s11340-008-9161-1
[26] López-Crespo, P., Burguete, R. L., Patterson, E. A., Shterenlikht, A., Withers, P. J., & Yates, J. R. (2008). Study of a Crack at a Fastener Hole by Digital Image Correlation, Experimental Mechanics, 49(4), pp. 551–559. DOI:10.1007/s11340-008-9161-1
[27] De-Matos, P.F.P., Nowell, D. (2009). Experimental and numerical investigation of thickness effects in plasticity-induced fatigue crack closure, International Journal of Fatigue, 31, pp. 1795–1804.
[28] López-Crespo, P., et al. (2009). Some experimental observations on crack closure and crack-tip plasticity, Fat. Fract. Eng. Mater, Struct.; 32, pp. 418-429
[29] Lopez-Crespo, P., Shterenlikht, A., Yates, J.R., Patterson, E. A., & Withers, P. J. (2009). Some experimental observations on crack closure and crack-tip plasticity, Fatigue & Fracture of Engineering Materials & Structures, 32(5), pp. 418–429. DOI:10.1111/j.1460-2695.2009.01345.x
[30] Lopez-Crespo, P., Shterenlikht, A., Yates, J.R., Patterson, E.A., & Withers, P.J. (2009). Some experimental observations on crack closure and crack-tip plasticity, Fatigue & Fracture of Engineering Materials & Structures, 32(5), pp. 418–429. DOI:10.1111/j.1460-2695.2009.01345.x
[31] Backman, D., Cowal, C., Patterson, E. (2010). Analysis of the effects of cold expansion of holes using thermoelasticity and image correlation, Fatigue & Fracture of Engineering Materials & Structures, 33, pp. 859–870.
[32] Mathieu, F., Hild, F., Roux, S. (2012). Identification of a crack propagation law by digital image correlation, International Journal of Fatigue, 36, pp. 146-154.

[33] Mathieu, F., Hild, F., Roux, S. (2013). Image-based identification procedure of a crack propagation law, Engineering Fracture Mechanics, 103, pp. 48-59.
[34] Zanganeh, M., Lopez-Crespo, P., Tai, Y.H., Yates, J.R. (2013). Locating the crack tip using displacement field data: a comparative study, Strain, 49, pp. 102–115.
[35] Yusof, F., Lopez-Crespo, P., Withers, P.J. (2013). Effect of overload on crack closure in thick and thin specimens via digital image correlation, International Journal of Fatigue, 56, pp. 17–24.
[36] Lopez-Crespo, P., Withers, P. J., Yusof, F., Dai, H., Steuwer, A., Kelleher, J. F., & Buslaps, T. (2012). Overload effects on fatigue crack-tip fields under plane stress conditions: surface and bulk analysis, Fatigue & Fracture of Engineering Materials & Structures, 36(1), pp. 75–84. DOI:10.1111/j.1460-2695.2012.01670.x
[37] Withers, P. J., Lopez-Crespo, P., Mostafavi, M., Steuwer, A., Kelleher, J., Buslaps, T. (2015). 2D mapping of plane stress crack-tip fields following an overload, Frattura ed Integrità Strutturale, 33, pp. 151-158. DOI: 10.3221/IGF-ESIS.33.19
[38] Lopez-Crespo, P., Moreno, B., Lopez-Moreno, A., Zapatero, J. (2015). Characterisation of crack-tip fields in biaxial fatigue based on high-magnification image correlation and electro-spray technique, International Journal of Fatigue, 71, pp. 17–25.
[39] Vasco-Olmo, J.M., Díaz, F.A., Patterson, E.A. (2016). Experimental evaluation of shielding effect on growing fatigue cracks under overloads using ESPI, International Journal of Fatigue, 83, pp. 117–126.
[40] Mokhtarishirazabad, M., Lopez-Crespo, P., Moreno, B., Lopez-Moreno, A., & Zanganeh, M. (2017). Optical and analytical investigation of overloads in biaxial fatigue cracks. International Journal of Fatigue, 100, pp. 583–590. DOI: 10.1016/j.ijfatigue.2016.12.0
[41] Mokhtarishirazabad, M., Lopez-Crespo, P., Moreno, B., Lopez-Moreno, A., & Zanganeh, M. (2016). Evaluation of crack-tip fields from DIC data: A parametric study. International Journal of Fatigue, 89, pp. 11–19. DOI:10.1016/j.ijfatigue.2016.03.0
[42] Elias Ferreira, S., Tupiassú Pinho de Castro, J., Antonio Meggiolaro, M. (2017). Using the strip-yield mechanics to model fatigue crack growth by damage accumulation ahead of the crack tip, International Journal of Fatigue, 103, pp. 557–575, DOI: 10.1016/j.ijfatigue.2017.06.039.
[43] Elias Ferreira, S., Tupiassú Pinho de Castro, J., Antonio Meggiolaro, M. (2018). Fatigue crack growth predictions based on damage accumulation ahead of the crack tip calculated by strip-yield procedures, International Journal of Fatigue, 115, pp. 89-106. DOI: 10.1016/j.ijfatigue.2018.03.001.
[44] Matvienko, Yu. G., Pisarev, V.S., Eleonsky, S.I. (2019). The effect of low-cycle fatigue parameters on damage accumulation near a hole, Engineering Failure Analysis, 106, 104175. DOI: 10.1016/j.engfailanal.2019.104175.
[45] Matvienko, Yu.G., Pisarev, V.S., Eleonsky, S.I. (2021). Evolution of fracture mechanics parameters relevant to narrow notch increment as a measure of fatigue damage accumulation. International Journal of Fatigue, 149, 106310. DOI: 10.1016/j.ijfatigue.2021.106310.
[46] Matvienko, Yu.G., Pisarev, V.S., Eleonsky, S.I. (2022). Low-cycle fatigue damage accumulation near the cold-expanded hole by crack compliance data, International Journal of Fatigue, 155, 106590. DOI: 10.1016/j.ijfatigue.2021.106590.
[47] Matvienko, Yu.G., Pisarev, V.S., Eleonsky, S.I. (2022). Quantification of low-cycle fatigue damage accumulation in stress concentration area by local strain evolution, Procedia Structural Integrity, 41, p. 192–198.
[48] Pisarev, V.S., Odintsev, I.N., Eleonsky, S.I., Apalkov, A.A. (2018). Residual stress determination by optical interferometric measurements of hole diameter increments, Optics and Lasers in Engineering, 110, pp. 437–456, DOI: 10.1016/j.optlaseng.2018.06.022.
[49] Matvienko, Yu.G., Pisarev, V.S., Eleonsky, S.I., Zaitsev, M.D. (2022). Damage accumulation near the cold-expanded hole due to high-cycle fatigue by crack compliance method, Frattura ed Integrita Strutturale; 59, pp. 115-128, DOI: 10.3221/IGF-ESIS.59.09.
[50] Haghshenas, A., Khonsari, M.M. (2017). Damage Accumulation and Crack Initiation Detection Based on the Evolution of Surface Roughness Parameters, International Journal of Fatigue; 107, pp. 130-144. DOI: 10.1016/j.ijfatigue.2017.10.009.
[51] Efthymiadis, P., Pinna, C., Yates, J.R. (2019). Fatigue crack initiation in AA2024: A coupled micromechanical testing and crystal plasticity study, Fatigue & Fracture Engineering Materials & Structures, 42, pp. 321–338. DOI: 10.1111/ffe.12909.